Verifying the Elastic Cross Section for a 5-10 GeV H(e,e')p Scattering Experiment at Jefferson Lab

A thesis presented to

the faculty of

the College of Arts and Sciences of Ohio University

In partial fulfillment

of the requirements for the degree

Bachelor of Science

Riley Reedy

May 2024

This thesis titled

Verifying the Elastic Cross Section for a 5-10 GeV H(e,e')p Scattering Experiment at Jefferson Lab

by

RILEY REEDY

has been approved for

the Department of Physics and Astronomy

and the College of Arts and Sciences by

Julie Roche

Professor of Physics

David Tees

Departmental Honors Coordinator

Randy Price

Assistant Dean of Arts and Sciences

Abstract

REEDY, RILEY, B.S., May 2024, Physics

Verifying the Elastic Cross Section for a 5-10 GeV H(e,e')p Scattering Experiment at Jefferson Lab (46 pp.)

Director of Thesis: Julie Roche

Nuclear cross section is a tool used by physicists to characterize scattering interactions between particles. It relates the probability of a reaction occurring to an effective "size" of the target particle's cross sectional area [1]. For electron-nucleon collisions, the elastic cross section values are well supported by experimental evidence for a wide range of Q^2 measurements. Because of this, comparing one's own experimental data to the known values can highlight possible issues with the data collection process. This makes elastic cross section an effective tool to safeguard against oversights when analyzing more complex interactions. This project analyzed elastic data from the Pion LT experiment run at Jefferson Lab in 2021-2022. Using the scattering analysis software ROOT and Jefferson Lab's Monte Carlo simulator SIMC, the measured elastic cross sections were able to be verified to the 10% level of their expected values.

Dedication

To my dog, Bento

Acknowledgments

I'd really like to thank my advisor Julie Roche for helping me through this process. She's been an amazing mentor and someone I'm grateful to have worked with and gotten to know. She created a very positive research experience for me and helped me grow a lot as an experimental physicist. I'd also like to thank my partner, who has been very kind, patient, and incredibly helpful not only in working on this thesis, but with everything I do. And finally, much appreciation to my friends and family for all their love and support!

Table of Contents

List of Tables

List of Figures

1 Introduction

1.1 Jefferson Lab

The Thomas Jefferson National Accelerator Facility (TJNAF), also known as Jefferson Lab and JLab, located in Newport News, Virginia, has been running medium energy nuclear experiments since 1994 [2]. An areal view of its campus is shown in Fig. 1.1. Its CEBAF accelerator is uniquely equipped to study the strong force with high levels of precision. The strong force is responsible for holding together the quarks found in protons and neutrons, both also called nucleons. Using CEBAFs high energy electron beam we can probe inside these nucleons to better understand their structure.

Figure 1.1: An aerial view of Jefferson Lab

[3]

1.2 Motivation

At low collision energies, electrons and protons preferentially interact elastically through the electromagnetic force. In this reaction, electrons bounce off the proton as a whole and kinetic energy is conserved in the system, see Fig. 1.2a. As energies increase however, the collisions start to favor inelastic reactions, where some of the energy is converted into creating new particles. At very high energies, the electrons are interacting

with a single quark inside the proton, in a process called Deep Inelastic Scattering (DIS). By studying DIS we can learn more about the strong force and the role quarks play in the structure of the proton.

(a) Elastic Reaction

(b) Inelastic Reaction

Figure 1.2: Types of collisions between a proton (p) and an electron (k): elastic collision on the left and one possible inelastic collision on the right.

[4]

Elastic reactions can tell us about the spacial distribution of nucleons, and they also play an important role in the data analysis process. Electron-proton elastic collisions have been well studied experimentally, and their cross sections are known for a wide range of energies to the few percent level. Comparing one's own elastic data to the known cross sections can highlight possible issues with one's data collection process. This has proven to be an effective tool to safeguard against oversights before analyzing one's inelastic data. Such an analysis is the topic of this thesis.

1.3 Experiment Summary

In 2021-2022 JLab's Hall C ran an experiment called Pion LT. The Pion LT experiment was approved for two studies: 1) The measurement of the charged pion form factor to high momentum transfer, and 2) a scaling study for the L-T separated pion

electroproduction cross section [5], where L (longitudinal) and T (transverse) describe the polarization of the virtual photon exchanged between the electron and the proton during the collision. In this experiment the high energy electron beam, adjusted between 5 GeV and 10 GeV, was incident on liquid cryogenic targets and the scatterings were recorded for hundreds of runs [1]. These studies used the outcomes of these collisions to study the strong force and the structure of nucleons.

Elastic scattering was also measured in order to cross-check the overall experimental setup. In this thesis I present an analysis of the elastic data at the 10% level. For the main analysis, the Pion LT collaboration analyze the data at the 1-2% level.

[1] Data taken with specific settings [beam energy, HMS angle, HMS momentum, target, ect...] for a short amount of time (around one hour) is called a run.

2 Background

This analysis compares the cross section of the experimental results to the Rosenbluth formula for the elastic cross section. This required using the experimentally measured kinematics of the electron to reconstruct the kinematics for the proton. This section defines the geometric cross section and how it relates to the number of detected events, and then covers the Rosenbluth formula for theoretical electron-proton elastic cross section. It also uses four-vector momenta to derive the proton's kinematics from the electron's kinematics.

2.1 Geometric Cross Section

In high energy scattering experiments, the outcome of a collision cannot be known before it happens. This uncertainty is governed by quantum mechanics, which describes these reactions in terms of their probability of occurring. The nuclear cross section acts as a means to interpret this probability.

The cross section (σ) is a cross-sectional area that measures the effective size of the target particle. It is proportional to a reaction's probability of occurring, so the more likely the event, the larger the area [1]. There are many possible reactions, and the total cross section is broken down into its elastic and inelastic components.

$$\sigma_{tot} = \sigma_{el} + \sigma_{inel}. \tag{2.1}$$

The inelastic component can be further broken down into its individual reactions. For a fixed target experiment, the cross section is largely a function of the incident particle's energy, and its scattering angle.

The standard unit for measuring cross section is in barns or millibarns. For reference, the elastic cross section for ep $\rightarrow$ ep scattering is roughly 10^{-7} barns for a 5 GeV electron beam energy.

$$1 \text{ barn} = 1 \text{ b} = 10^{-28} \text{ m}^2 = 10^{-24} \text{ cm}^2$$

$$1 \text{ millibarn} = 1 \text{ mb} = 10^{-31} \text{ m}^2 = 10^{-27} \text{ cm}^2$$

2.1.1 Geometric Cross Section

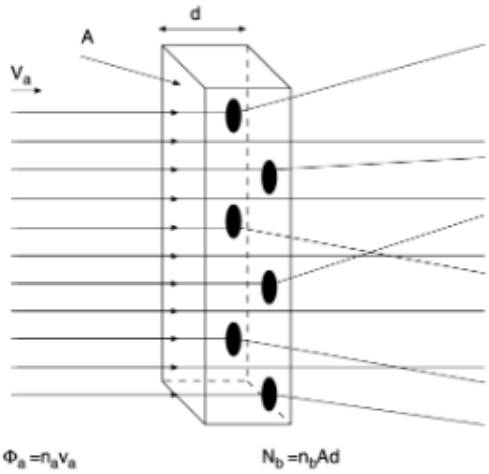

Figure 2.1: This is a physical example of geometric cross section. The beam is incident from the left and hits a target, scattering off the [black circular] particles inside. These target particles have a cross section of σ.

[1]

The geometric cross section is an approximation for the experimental cross section, see Fig. 2.1. Total cross section is generally defined as

$$\sigma = \frac{number\ of\ reactions\ per\ unit\ time}{beam\ particles\ per\ unit\ time\ per\ unit\ area \times\ scattering\ centers}$$

where,

- **Number of reactions per unit time** is the rate of events picked up by the detector, $\dot{N}_{events}$.

- **Beam particles per unit time per unit area** is the beam flux,

$$\Phi_{beam} = \frac{\dot{N}_{beam}}{A} \tag{2.2}$$

where $\dot{N}_{beam}$ is the rate of incident beam particles, and A is the beam's area.

- **Scattering centers** is the number of atoms in the target,

$$N_{tar} = n_{tar} A d, \tag{2.3}$$

where n_{tar} is the density, A is the cross sectional area, and d is the target thickness.

Therefore

$$\sigma = \frac{\dot{N}_{events}}{\Phi_{beam} N_{tar}} = \frac{N_{events}}{N_{beam} n_{tar} d} \tag{2.4}$$

.

The two A values from the beam and target are able to cancel because the beam's spread is smaller than the target's area. Also, the time component is cancelled from both N and N_{beam}, since the "rate" is considered to be over the same time period for both.

Equation 2.4 will need to be adjusted since the detectors only take up a small section of potential scattering space, called the solid angle $\Delta\Omega$ as shown in Fig. 2.2.

$$\Delta\Omega = \frac{A_D}{r^2} \tag{2.5}$$

which uses surface area of the detector A_D and distance from the target to the detector r. Solid angle is in units of sterradians. Dividing the cross section in Equation 2.4 by the solid angle creates a differential cross section dependent on Ω.

$$\frac{d\sigma}{d\Omega} = \frac{N_{events}}{N_{beam} n_{tar} d} \frac{1}{\Delta\Omega} \tag{2.6}$$

For elastic scattering, $\frac{d\sigma}{d\Omega}$ is well described by the Rosenbluth formula.

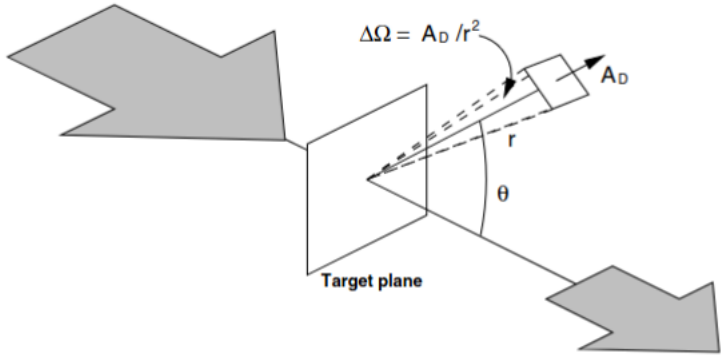

Figure 2.2: The beamline is shown with two arrows as it goes through the target plane. Only particles that are scattered into the detector's solid angle are captured and counted.

[1]

2.1.2 The Rosenbluth formula for Cross Section

To start, we will use the Rutherford cross section for an electron scattering off of an electrically charged, spinless, point-like particle [1].

$$\left(\frac{d\sigma}{d\Omega}\right)_{Rutherford} = \frac{4Z^2\alpha^2(\hbar c)^2E'^2}{|\mathbf{q}c|^4}, \tag{2.7}$$

where E' is the electron's scattered energy, q is the momentum transferred to the proton, Z is the atomic number (1 for the proton), and α is the fine structure constant. This equation does not consider recoil, or the electron's spin. These adjustments are however seen with the Mott cross section.

To consider spin but not recoil, the equation is

$$\left(\frac{d\sigma}{d\Omega}\right)^*_{Mott} = \left(\frac{d\sigma}{d\Omega}\right)_{Rutherford} \cdot \left(1 - \beta^2 sin^2\left(\frac{\theta}{2}\right)\right) \tag{2.8}$$

where θ is the electron's scattering angle, and $\beta = v/c$ is the relativistic beta for the electron. Since in high energy experiments $v \approx c, \beta \rightarrow 1$ and Equation 2.8 becomes approximately

$$\left(\frac{d\sigma}{d\Omega}\right)^{*}_{Mott} \approx \left(\frac{d\sigma}{d\Omega}\right)_{Rutherford} \cdot \left(\cos^2\left(\frac{\theta}{2}\right)\right). \tag{2.9}$$

To consider recoil off the proton, the cross section must be adjusted by the ratio of the electron's scattered (E') to incident energy (E)

$$\left(\frac{d\sigma}{d\Omega}\right)_{Mott} = \left(\frac{d\sigma}{d\Omega}\right)^{*}_{Mott} \cdot \left(\frac{E'}{E}\right). \tag{2.10}$$

The Rosenbluth formula describes the cross section for an electron scattering off a nucleon. Nucleons are non point-like, and have a current and charge distributions that affect scattering at extended distances. These distributions are taken into account using two form factors, one for the current ($G_M(Q^2)$) and one for the charge ($G_E(Q^2)$) called the electric and magnetic form factors respectively. Q^2 is the momentum transfer squared between the electron and the proton

$$Q^2 = -4pp' \sin^2\left(\frac{\theta}{2}\right) \tag{2.11}$$

where p is the beam energy, p' is the scattered electron energy, and θ is the scattered electron angle as seen in Fig. 2.3.

These form factors have been measured experimentally for a wide range of Q^2 largely by experiments run in the 1960's and 1970's [1]. The fact that the nucleon form factors have been extensively measured is the reason comparing one's own elastic cross section against it is so effective as a check against experimental errors.

In Fig. 2.3, **q** is a measure of the amount of momentum transferred from the electron to the proton. This is represented by a virtual photon as the force carrier between the two

particles. For small Q^2 values, the electron effectively sees a point particle, but at much higher momenta the spacial distribution is no longer inconsiderable. The virtual photon's wavelength, governed by the electron's momentum, is directly related to how well the electron is able to resolve the proton's structure. This is shown by how the form factors behave as a function of Q^2 as seen in Fig. 2.4. It was experimentally found that for protons, both G_E and G_M fall off with increasing Q^2. As such they're able to be combined into a single term that describes both, the dipole form factor G^{dipole}.

$$G^{dipole}(Q^2) = G_E(Q^2) = \frac{G_M}{2.79}(Q^2) \tag{2.12}$$

The Rosenbluth formula (Equation 2.13) corrects the Mott cross section by using these form factors to approximate the spacial distribution of the proton at high Q^2.

$$\left(\frac{d\sigma}{d\Omega}\right) = \left(\frac{d\sigma}{d\Omega}\right)_{Mott} \cdot \left[\frac{G_E^2(Q^2) + \tau G_M^2(Q^2)}{1+\tau} + 2\tau G_M^2(Q^2)\tan^2\left(\frac{\theta}{2}\right)\right] \tag{2.13}$$

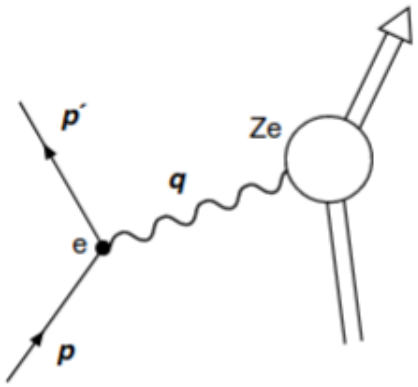

Figure 2.3: A Feynman Diagram for an electron scattering off a charge distribution

[1]

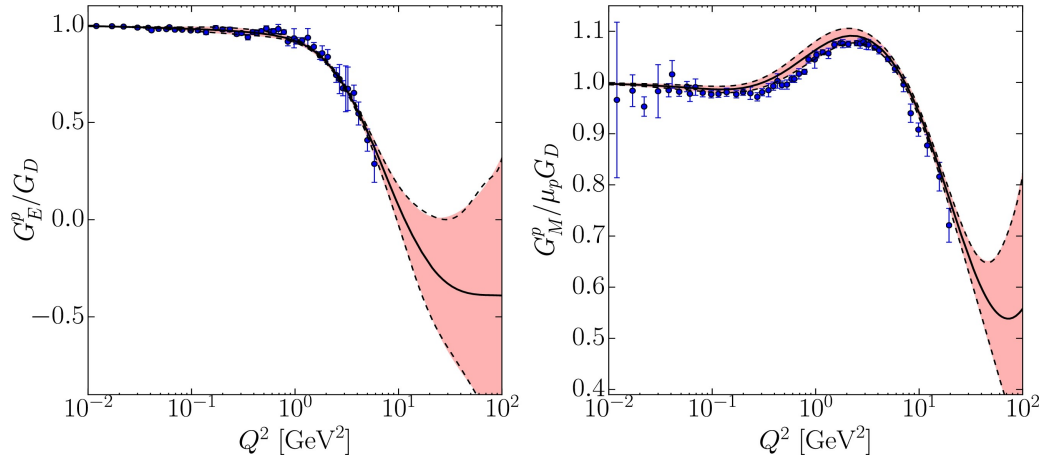

Figure 2.4: G_E and G_M form factor values for a range of Q^2 shown for the proton [6]

2.1.3 Elastic Kinematics

In two-body elastic collisions ($A + B \rightarrow A + B$), the kinematics of the reactions are totally defined by only two quantities. For instance, the incident particle's energy and scattering angle are two useful values for reconstructing collisions because they can be accurately measured by the accelerator. The derivation of this is done using four-momentum vectors since high energy collisions happen at close to the speed of light. Four-momentum is defined as

$$\overline{p}(x_o, x_1, x_2, x_3) = (E/c, \mathbf{p}), \tag{2.14}$$

where $\mathbf{p}$ is the three-vector, and

$$\overline{p}^2 = E^2/c^2 - \mathbf{p}^2. \tag{2.15}$$

The relativistic energy-momentum relation is

$$E^2 = \mathbf{p}^2 + (mc^2)^2. \tag{2.16}$$

From the frame of reference where the electron is at rest, $\mathbf{p} = 0$ and

$$m = \sqrt{\overline{p}^2}/c \tag{2.17}$$

by Equation 2.15 and Equation 2.16. "m" is called the "invariant mass" of the particle.

Consider a high energy electron scattering off a proton with four-momenta $\overline{p}$ and $\overline{P}$ respectively. Conservation of energy and momentum states that

$$\overline{p} + \overline{P} = \overline{p}' + \overline{p}' \tag{2.18}$$

squaring this gives,

$$(\overline{p} + \overline{P})^2 = (\overline{p}' + \overline{P}')^2 \rightarrow \overline{p}^2 + 2\overline{p}\overline{P} + \overline{P}^2 = \overline{p}'^2 + 2\overline{p}'\overline{P}' + \overline{P}'^2. \tag{2.19}$$

Since in elastic scattering, the invariant masses stay the same for both particles (m_e for the electron and M for the proton), using Equation 2.17, so do their four-momenta squared, such as

$$\overline{p}^2 = \overline{p}'^2 = m_e^2 c^2. \tag{2.20}$$

To get the electron's scattered energy, start with the dot product of the four-momenta

$$\overline{p} \cdot \overline{P} = \overline{p}' \cdot \overline{P}'. \tag{2.21}$$

Using Equation 2.20 and Equation 2.21 and distributing the $\overline{p}'$ through:

$$\overline{p} \cdot \overline{P} = \overline{p}' \cdot (\overline{p} + \overline{P} - \overline{p}') = \overline{p}\overline{p}' + \overline{p}'\overline{P} - m_e^2 c^2. \tag{2.22}$$

To isolate the relevant E', assume the laboratory frame of reference, where $\mathbf{P} = 0$.

$$E \cdot Mc^2 = E'E \cdot (1 - \cos(\theta)) + E' \cdot Mc^2 \tag{2.23}$$

and solve for E'

$$E' = \frac{E}{1 + E/Mc^2 \cdot (1 - \cos(\theta))}. \tag{2.24}$$

The proton's kinematics can then be found using the classical conservation of momentum equations.

$$|\mathbf{p}| = |\mathbf{p}'| \cos(\theta_e) + |\mathbf{P}'| \cos(\theta_p) \tag{2.25}$$

and

$$|\mathbf{p}'| \sin(\theta_e) = |\mathbf{P}'| \sin(\theta_p). \tag{2.26}$$

Combining and solving for θ_p yields

$$\theta_p = \arctan\left(\frac{|\mathbf{p}| \sin(\theta_e)}{|\mathbf{p}| - |\mathbf{p}'| \cos(\theta_e)}\right) \tag{2.27}$$

then $\mathbf{P}$ can be found with Equation 2.26.

The proton's kinematics are needed when configuring the simulation SIMC to create elastic reactions.

In inelastic electron-proton collisions, the invariant mass (see Equation 2.17) of the proton is no longer equal to the proton's rest mass. This is because some of the proton's scattered energy is converted into the mass and energy of the new particle(s). The proton's invariant mass is now called the missing mass, W.

In elastic collisions,

$$W^2 = \overline{P}'^2 = (\overline{p} + \overline{P} - \overline{p}')^2 = M\overline{p}^2 \tag{2.28}$$

which makes W equal to the mass of the proton (0.938 GeV/c^2). This is able to be calculated using only the electron's kinematics. In the case of inelastic scattering, W will be bigger than than M. This missing mass is used to distinguish between elastic and inelastic collisions in this analysis, see Section 4.3.3 and Fig. 4.5.

3 Experimental Methods

3.1 Description of Apparatus

3.1.1 CEBAF

The Continuous Electron Beam Accelerator Facility (CEBAF) at Jefferson Lab, shown in Fig. 3.1, has been used for the last 30 years to study the structure of hadronic matter. Since its most recent upgrade in 2016, the electron beam is capable of carrying a range of 0.4 - 12 GeV of energy. Beam currents range from 0.1 - 120 μA to Halls A and C, while B and D use currents in the nA range. The racetrack-style accelerator has a two linacs (North and South) that accelerate the beam, and two curved sections with steering magnets to connect them. The electron beam will circle the track up to 5 times to build up its energy before being directed to a target. [7] [8]

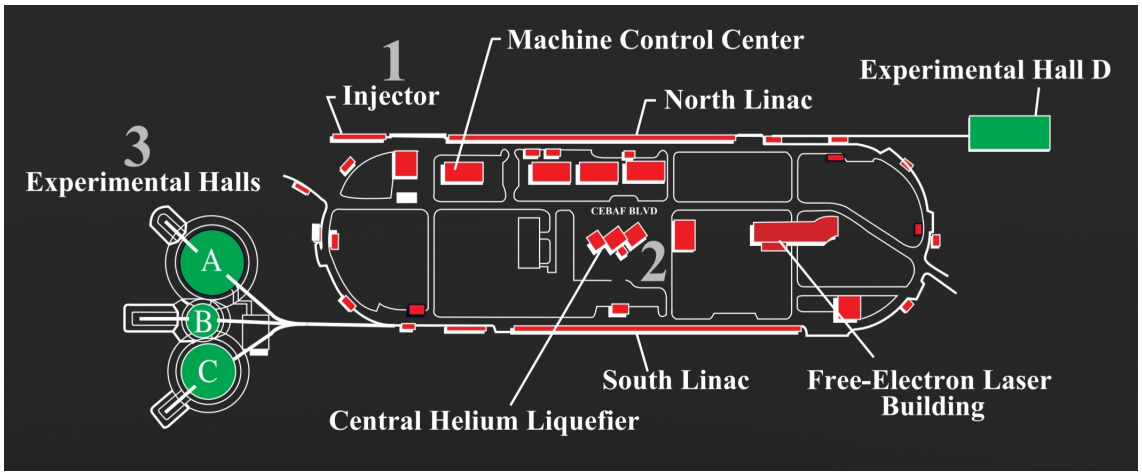

Figure 3.1: CEBAF at Jefferson Lab

[9]

CEBAF is a specialized accelerator in its ability to create a continuous electron beam. This is measured using a duty factor, which is the ratio of a beam's pulse duration to the time interval between pulses. A high duty factor corresponds to a more continuous beam.

This is preferred over a pulsed beam for coincidence experiments that measure rare processes since it suppresses accidental coincidence events. To create the continuous beam, each linac is equipped with 25 niobium Superconducting Radio Frequency (SRF) cavities. Each are submerged in a 2 K helium bath, well below niobium's superconductivity point. This reduces the Ohmic heating of the cavity, allowing a high energy beam to run continuously for long periods of time without overheating. [10]

3.1.2 Beamline

As the electrons leave the racetrack and move into Hall C, beam data is taken by detectors connected to radio frequency cavities. The polarimeter, as well as Beam Current Monitors (BCMs), Beam Position Monitors (BPMs), and wire scanners collect scaler data on the variables such as the beam's energy, position, and current. Beam energy data is collected with high accuracy as a side effect of needing to keep the beam centered in the pipe. This data is stored by the Data Acquisition System (DAQ).

The CEBAF is also specialized in its ability to create a polarized beam. It can currently polarize up to 88% of its electrons [11]. This is done by polarizing the source photon laser, which will affect the polarization of the photoelectrons it creates. For beam delivered in Hall C, the polarization is measured by a Moller polarimeter which sits at the beginning of Hall C beamline.

3.1.3 Hall C

3.1.3.1 The Detectors

Experimental Hall C houses two main detectors: the High Momentum Spectrometer (HMS) and the Super High Momentum Spectrometer (SHMS), shown in Fig. 3.2. They sit together on a circularly curved railroad track that allows them to adjust the angle of the detected particles. The HMS can move between $10.5° - 90°$, and the SHMS can move

between $5° - 40°$, with respect to the beamline. They're both covered by thick concrete shielding to protect their detectors from background radiation [12]. For the analysis presented in this document, only data from the HMS was used.

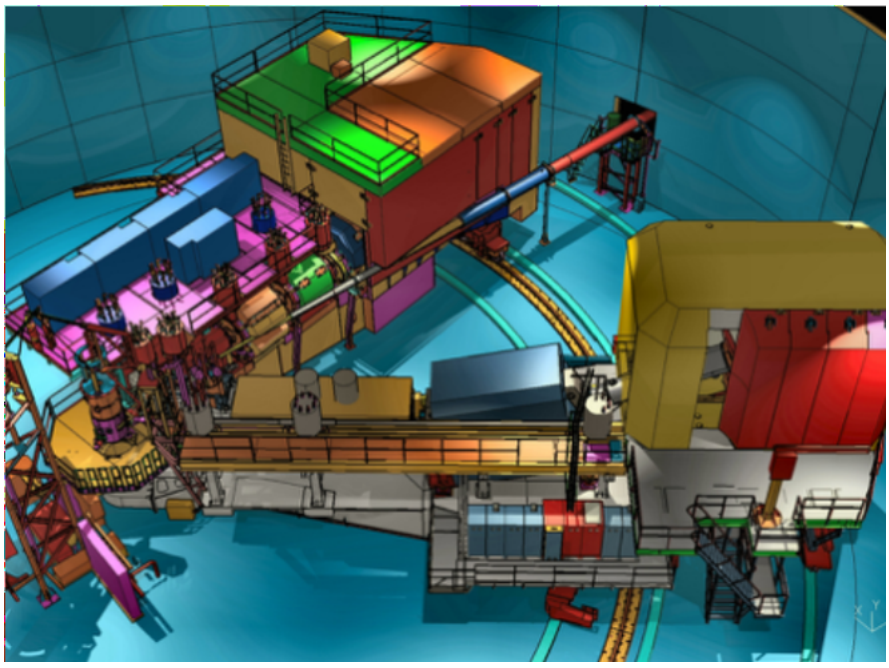

Figure 3.2: This is a Hall C illustration with the SHMS at the top of the arc, and the HMS at the bottom. Both are connected to the target chamber.

[12]

Spectrometers are devices able to filter data for a specific property. The HMS filters particles for momentum by using powerful superconducting magnets. These magnets create a gradient magnetic field that bends charged particles from the collisions towards their detectors at a curvature proportional to the particle's momentum. The HMS can select momenta ranging from $0.4 - 7.3$ GeV at a relative resolution of $1\text{x}10^{-3}$ and a $\pm 10\%$ acceptance. Looking at the HMS in Fig. 3.3, there are four spectrometer magnets connecting the scattering chamber to the detector hut. Three quadrupole magnets are

placed first to control the range of angles of the particles detected by the spectrometer. These are followed by a dipole magnet that bends the particles' trajectories upwards by 25° into the detector stack. Together the magnet defines the angular and momentum acceptance for the spectrometer [12], shown in Table 3.1.

Parameter	HMS
Momentum Range (GeV/C)	0.5 – 7.3
Momentum Acceptance (%)	±10
Momentum Resolution (%)	0.10 – 0.15
Horiz. Angle Acceptance (mrad)	±32
Horiz. Angle Resolution (mrad)	0.8
Vert. Angle Acceptance (mrad)	±85
Vert. Angle Resolution (mrad)	1.0
Solid Angle (mrad)	8.1
Maximum Scattering Angle	≤ 80°
Minimum Scattering Angle	≥ 10.5°
Vertex Reconstruction Resolution (cm)	0.3

Table 3.1: HMS Parameters

[13]

3.1.3.2 HMS Detector Stack

After the particles are filtered, they are sent into the detector stack. Fig. 3.4 shows the set of detectors used in the HMS. These perform specialized tasks in order to trigger, track, and identify the incoming particles.

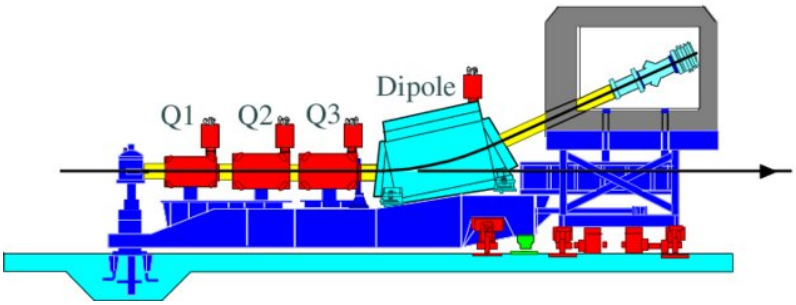

Figure 3.3: HMS Magnets

[14]

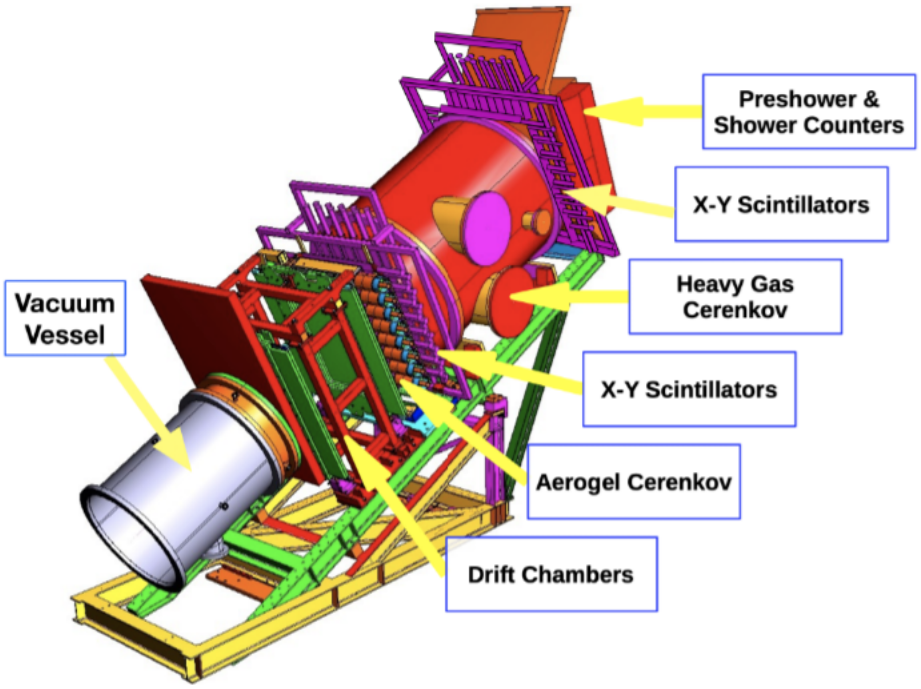

Figure 3.4: HMS detector stack

[15]

Drift Chambers The Drift chambers are located at the front of the stack, after the vacuum chamber. Wire planes inside the drift chamber are able to pick up a signal

when charged particles pass through and ionize the gas in the detector. The excitation travels to the wires and ultimately the signals can be reconstructed to track momentum, position, and scattering angle.

Cherenkovs The Cherenkov detectors are able to identify charged particles by producing a signal depending on the mass of that particle. When a charged particle moves through its material at a speed greater than the speed of light in the material, it creates Cherenkov photons that are collected by PMTs. The material and its index of refraction can select which particles will produce Cherenkov light at a given momentum. Typically in the HMS, they will discriminate between electrons and pions.

Scintillating Hodoscopes These detectors are made up of long thin scintillating rods set up in a grid pattern that cover the range of acceptance. Scintillators are quick to produce a signal after being struck by an incoming particle. They trigger at the nano-second (ns) scale, as compared to the wire chambers which trigger in micro-seconds (μs). The signal is collected by PMTs which turn it into an electrical signal. Scintillators are mainly used as the trigger for the DAQ, but also serve as a way to track position and identify the particles.

Shower Counters The shower counters are last in the stack, and use thick lead glass calorimeters to absorb and detect the leftover energy. This can serve as a final way to discriminate the different incoming particles.

3.1.3.3 The Target

The beam is incident on a target ladder holding multiple targets for main data collection and calibration. This is shown in Fig. 3.5. The Loop targets are cryogenically cooled and are the main targets of the experiment. This includes the H_2 (LH2 or Loop 2)

liquid hydrogen used in the elastic analysis. The LH2 target is housed in a capsule-shaped aluminum (Al 7075) cell. The specifications for the LH2 target are in Table 3.2.

Other targets such as the “Dummy”, “Optics”, and “Carbon Hole” are used for calibration and analysis. The dummy target, used in the elastic analysis, is an empty shell used to account for the electrons that scatter off the cell walls. As such the dummy has a slightly thicker aluminum casing. This is also seen in Table 3.2.

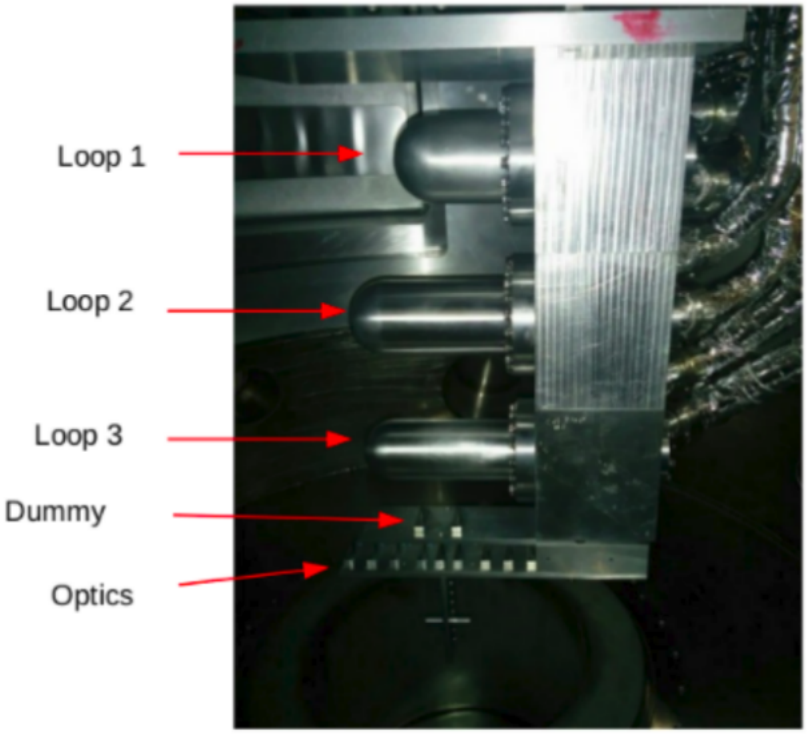

Figure 3.5: The target ladder that sits inside the scattering chamber

[16]

Target Type	Entrance (mm)	Exit (mm)	Length (mm)
H_2	0.150 ± 0.011	0.191 ± 0.019 Tip 0.219 ± 0.018 Wall	100 ± 0.26
Dummy	0.1703 ± 0.0002	0.1677 ± 0.0002	100

Table 3.2: Target Wall Thickness used for Pion LT

3.2 Data Aquisition

3.2.1 CODA

The CEBAF Online Data Acquisition (CODA) system is the program used to manage when and how the detector data is recorded [17]. It's able to be configured for data prescales and run type, in order to control the amount of data that gets stored out of the total interactions. When a detector in the HMS hut is triggered, it will signal a Read Out Controller (ROC) crate to begin taking data. This signal undergoes some preprocessing by an event builder before it's stored by CODA in the counting house. Depending on the design of the detector, the data is processed by one of three devices:

ADC Analog-to-digital converters measure how much energy is deposited into a detector over the given pulse window. These signals come from the calorimeters and the Cherenkov's PMTs.

TDC Time-to-digital converters measure time intervals called Time of Flight (TOF). They consist of a starting and stopping trigger which measure the time between the triggers. TDC signals are used in the drift chambers to measure position, and through the scintillators to measure speed.

Scaler Scalers record the accumulation of signals that occur too rapidly to be recorded individually. Because they only count, scalers have virtually zero dead

time. They can be used to collect data on the beam such as incoming current and helicity. They can also be used to measure dead time by comparing the data from the raw scalers, which collect data for the whole run, to the live scalers, which only count when the DAQ isn't occupied. [10]

3.2.2 HCANA

The Hall C Analyzer (HCANA) is a program that analyzes the data after it's been collected. In part, it calibrates each ADC and TDC signal to turn them into their physical quantities. By giving HCANA a specific run number and the number of events to be replayed, it will create a file that contains every event requested and information about the involved particles' kinematics.

Rootfiles and Trees: These replay files are created using ROOT [18], a C++/python framework used to analyze data from nuclear and particle experiments. This data is interfaced through rootfiles (.root). ROOT has a useful data structure called a tree that allows for each detected event to be saved in its own separate entry with all its kinematics. Thus, any tree object is able to hold up to all of the events for any run. This makes it easy to traverse through the events, and also to create histograms that analyze the variables for these events, called branches.

There are two coordinate systems of interest for a given collision: one with respect to the target (vertex), and one with respect to the detector (focal plane). A visual for this is found in Fig. 3.6. The detectors take data in the detector coordinate system, and HCANA reconstructs the kinematics at the target using an optics matrix. [19]

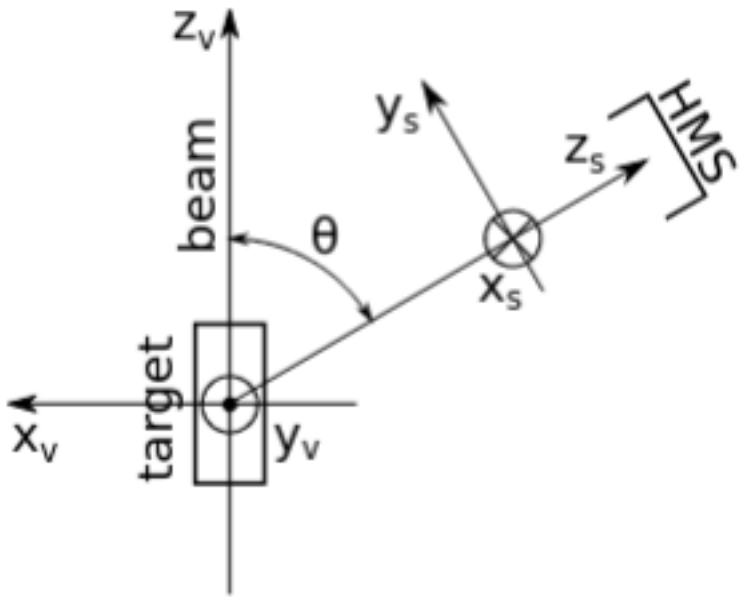

Figure 3.6: The target and HMS detector's relative coordinate systems

[19]

4 Analysis and Results

This analysis compares the Rosenbluth elastic cross section to the experimental elastic cross section with the goal of verifying each run's experimental value to be within 10% of its Rosenbluth value. The point-like Rosenbluth cross section was found by using the beam energy and scattering angle in Equation 2.13, and the measured cross section was found by selecting elastic data from the replay files and using the simulation package SIMC to take into account the extended detector and target effect. The analysis was done on three runs of varying energy and angle. The process is laid out here and the results are found in Table 4.3.

4.1 Obtaining the Central Kinematic Setpoints

Each of the runs I worked with were taken with a specific beam energy, HMS angle (θ) and HMS momentum. These conditions are documented in an electronic logbook [20] as well as in Table 4.1. They are used in the Rosenbluth cross section calculation (see Equation 2.13.)

Run Number	E_{beam} (GeV)	HMS θ (deg)	HMS Momentum (GeV/c)
12080	9.158	19.880	5.900
12083	9.158	19.880	5.900
13854	7.913	19.885	5.202

Table 4.1: Logbook kinematics for Runs 12080, 12083, and 13854

4.2 Beam Charge Evaluation

During any run, it's not unusual for the electron beam to trip, meaning that current will drop to zero for upwards of a few seconds. Although a single trip is small, multiple

trips in the run can grossly overestimate the amount of charge hitting the target. For this reason we make cuts to the data around these beam trips. This is done by defining a course cutoff of current for each run of 1 μA, and resumming the scaler charge data without the trips.

4.3 Selecting Elastic Electrons in the HMS

To select good data, "cuts" can be placed on a variable to filter out any events that fall outside a specified range. This effect happens to all events in the run, hiding the unwanted events from the analysis process.

4.3.1 Good Track Cuts

It's important for the events that are selected to be close to the central kinematics of the detector in terms of position and momentum. This selection avoids events that may have been too close to the detector's walls or edge of the magnets.

Momentum Acceptance: Δp (H.gtr.dp) measures, as a percentage, how deviated the momentum of the scattered electron is to the central momentum of the spectrometer. This filters out events where the electron is too close to the spectrometer wall. This was cut made at 8% shown in Fig. 4.1.

X and Y Position: The particle's position in the detector comes from the drift chambers. Cutting this is another check that the electron isn't too close to the detector's edges. Similarly to Δp, the variables H.dc.xp and H.dc.yp are angles of deviation from the central angle θ. x was cut at 0.08, and y was cut at 0.045. This is shown in Fig. 4.2.

4.3.2 Particle Identification

For this data, the elastic electron is expected to be picked up by the HMS, and the elastic proton goes undetected. To discriminate the electron from other particles (eg. π^-)

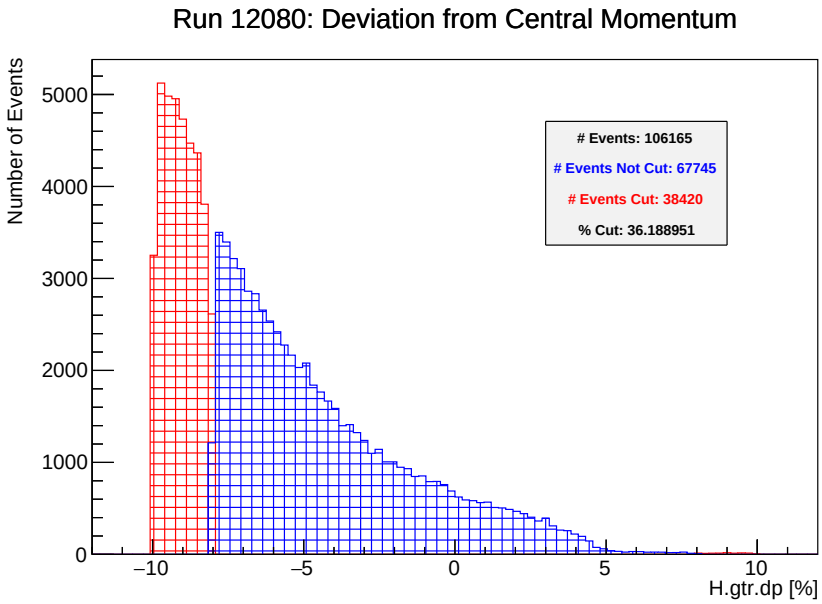

Figure 4.1: Run 12080 H.gtr.dp cut

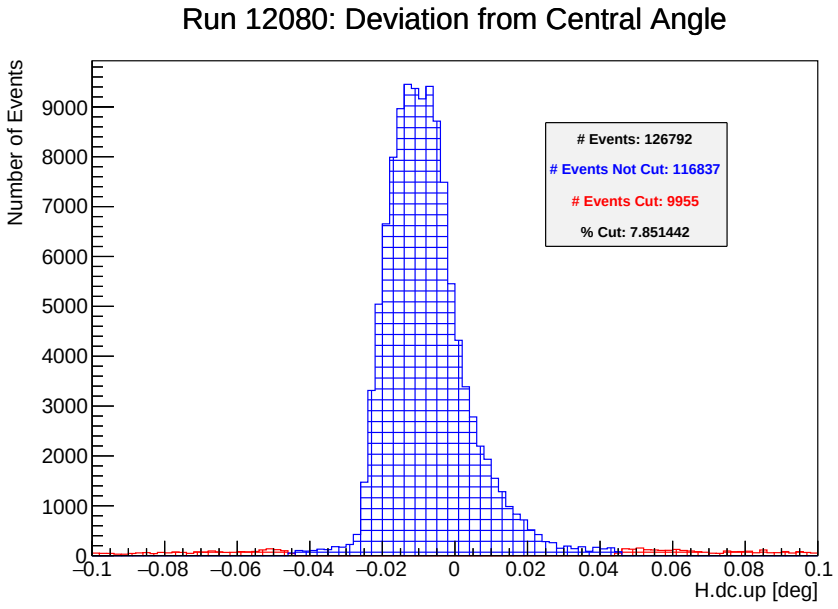

Figure 4.2: Run 12080 H.dc.yp cut

that may have come from inelastic collisions, the Cherenkov and hodoscope detectors in the HMS are used.

Cherenkov Selection: In the Cherenkov detectors, light is created by particles that travel faster than the speed of light in that material. The material in the HMS for Pion LT is chosen such that the electron produces a small signal while pions produce close to none. To ensure that the charged particle that went through the HMS was an electron, a cut of > 1.5 photoelectrons was set, shown in Fig. 4.3.

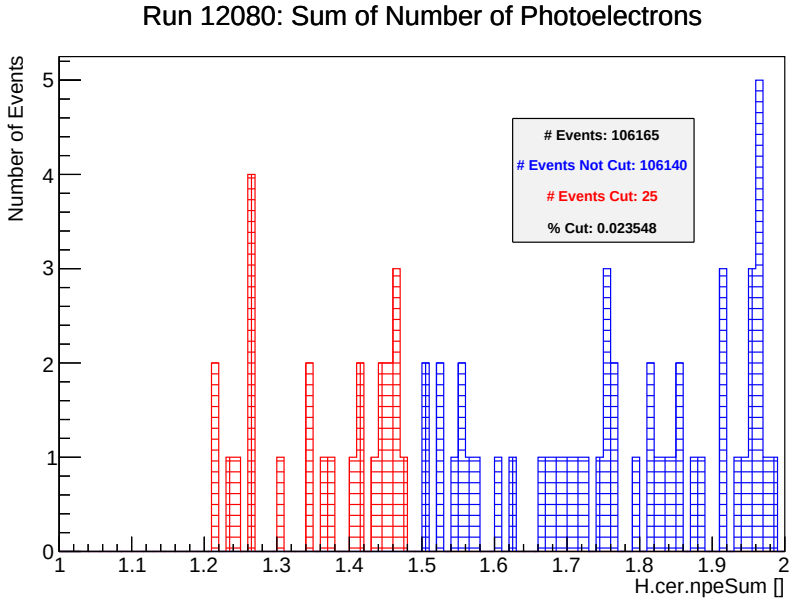

Figure 4.3: Run 12080 H.cer.npeSum cut

Beta: Relativistic beta (β) is the ratio of a particle's speed v to c. Some particles, such as the pion, are significantly heavier than the electron, but can still be filtered by the same momentum. These particles will have a much lower speed than the electron. The electron is much lighter making its speed very close to c, so β was cut for 1.0±0.3, shown in Fig. 4.4.

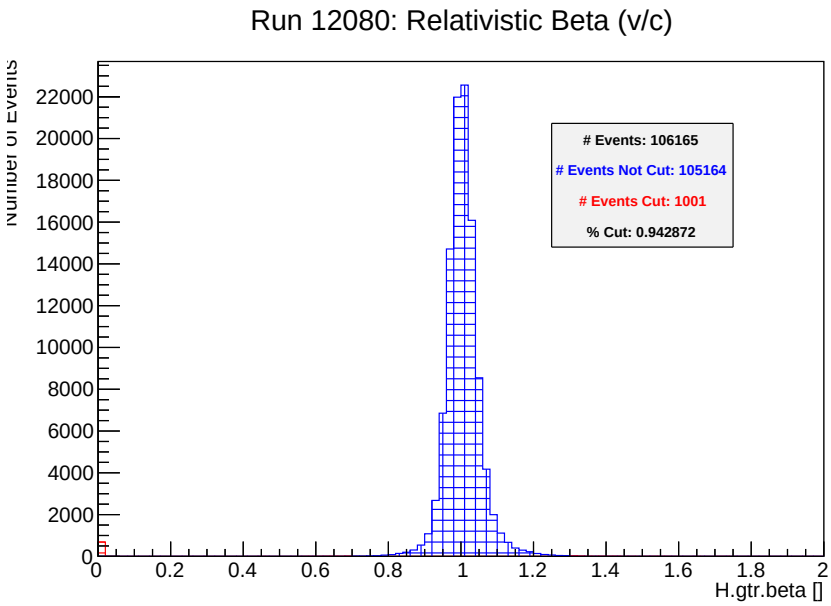

Figure 4.4: Run 12080 H.gtr.beta cut

4.3.3 Elastic Scattering

Missing Mass: Missing mass is a value associated with the momentum transfer (q^2) from the incoming electron, to virtual photon emitted by the collision. For elastic events, this missing mass will be exactly around the mass of the proton, since no momentum is transferred elsewhere. This cut was made so that events outside of ±0.040 GeV/c^2 of the known mass (0.938 GeV/c^2) were rejected, effectively filtering for only elastic collisions, shown in Fig. 4.5.

4.4 Prescales and Dead Time

When an event is detected by the scintillators, the DAQ is triggered to start recording detector data. This process leaves the system temporarily blind to any events that may trigger in that time. This is called the dead time. To minimize dead time, and to control the rate of input data, prescales can be set. The prescales, configurable with CODA before

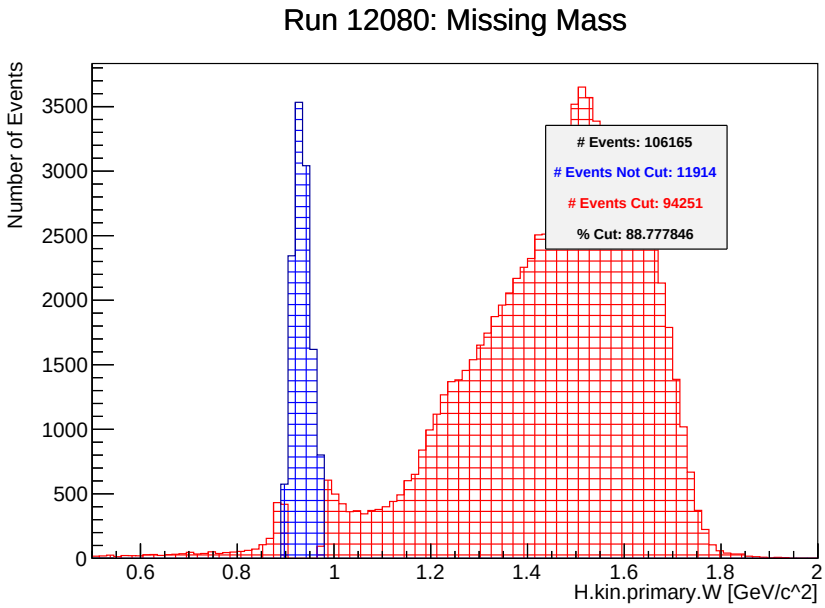

Figure 4.5: Run 12080 H.kin.primary.W cut

each run, adjust the DAQ to process and save a fraction of the total events that were triggered. [16]

The equation to calculate the scale factor from the prescale value is

$$\textbf{Scale Factor} = 2^{Prescale-1} + 1, \tag{4.1}$$

which results in the suppression factors listed in Table 4.2.

To retrieve the true input rate, the number of events saved is multiplied by the scale factor.

4.5 Background Correction

The aluminum housing for the LH2 target, while thin, still interacts with the electron beam. These collisions cause an overestimation of the number of events that occurred. To correct for this, the targets are periodically swapped out for hollow dummies and runs are taken considering only the casing. This data can be used to correct the true number of

Prescale Value	Scale Factor	Example
0	1	100 kHz → 100000 Hz
1	2	100 kHz → 50000 Hz
2	3	100 kHz → 33333 Hz
3	5	100 kHz → 20000 Hz
4	9	100 kHz → 11111 Hz
5	17	100 kHz → 5882 Hz
6	33	100 kHz → 3030 Hz
7	65	100 kHz → 1538 Hz

Table 4.2: Prescales applied to 100kHz input rate

events by subtracting out the dummy data. Fig. 4.6 shows the reconstructed scattering on the y-axis for a dummy target.

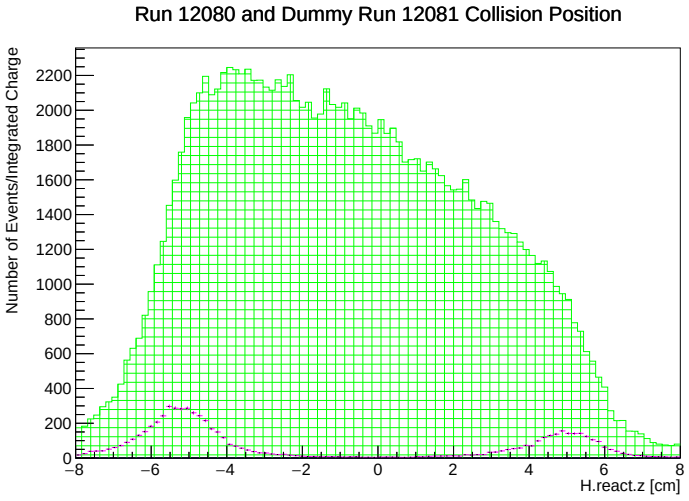

Figure 4.6: Run 12080 is in green and Run 12081 is in purple. This is the reconstructed z position of the collision from target frame.

4.6 Monte Carlo Simulation

Monte Carlo methods are a type of algorithm that use random sampling to estimate the possible outcomes of an uncertain event. Simulators built on Monte Carlo methods are particularly useful in nuclear and particle physics because they can be used to simulate experimental results of collision experiments, where outcomes are probabilistic.

SIMC [21] is a program developed specifically for simulating data that comes from Hall C at Jefferson Lab. Given run specifications as input, it can create simulated reactions and store them in the same style of rootfile as the replays. One can then apply cuts just the same as were done on the experimental data. One major benefit of using a simulation program is that it can be configured to account for radiative corrections and an extended target, see Fig. 4.7. SIMC's results are also based on the Rosenbluth cross section, but it is now a distribution based on varying beam energy and angle. Table 4.4 shows the difference in expected cross section when taking these into consideration. To configure the input file, the kinematics from both the proton and electron were needed. The electron kinematics from the electronic logbook [20] were used. A kinematics calculator [22] was used to get the proton's kinematics given the electron's.

4.7 Extracting the Cross Sections

After configuring SIMC to replicate each run and making cuts on those generated events, the SIMC cross section could be found from the *sigcc* tree variable, see Table 4.4.

Fig. 4.8, Fig. 4.9, and Table. 4.3 show that SIMC matches the experimental results in corrected number of events (events per unit charge) as well as shape. One discrepancy in the W value seen in Fig. 4.9 is that the peaks are offset. This is fixed by making a cut around their individual central values instead of the same cut for both. Table 4.3, shows that their events agree up to 93%.

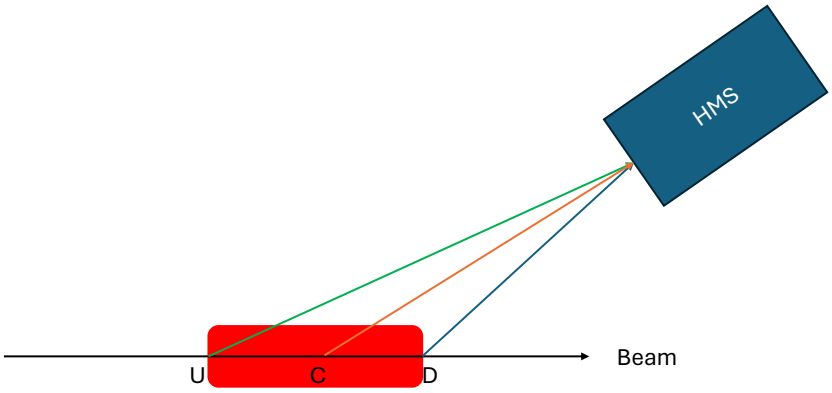

Vertex position	U (upstream)	C (center)	D (downstream)
Beam energy	E_U= nominal beam energy	$E_C<E_U$	$E_D<E_C<E_U$
Average scattered angle detected	$\theta_U<\theta_C$	θ_C= nominal spectrometer angle	$\theta_D>\theta_C$
Average distance vertex to spectrometer entrance	$r_U>r_C$	r_C= nominal	$r_D<r_C$

Figure 4.7: An extended target diagram, and how it affects beam energy and the electron's scattered angle

[23]

Run Number	$N_{measured}$	N_{SIMC}	Ratio
12080	12642	13021	.971
12083	11250	11210	1.00
13854	16875	18149	.930

Table 4.3: The results of the SIMC analysis are shown here. The ratio of the corrected number of events shows how far off the measured results are to the simulation. All the runs are within 10%.

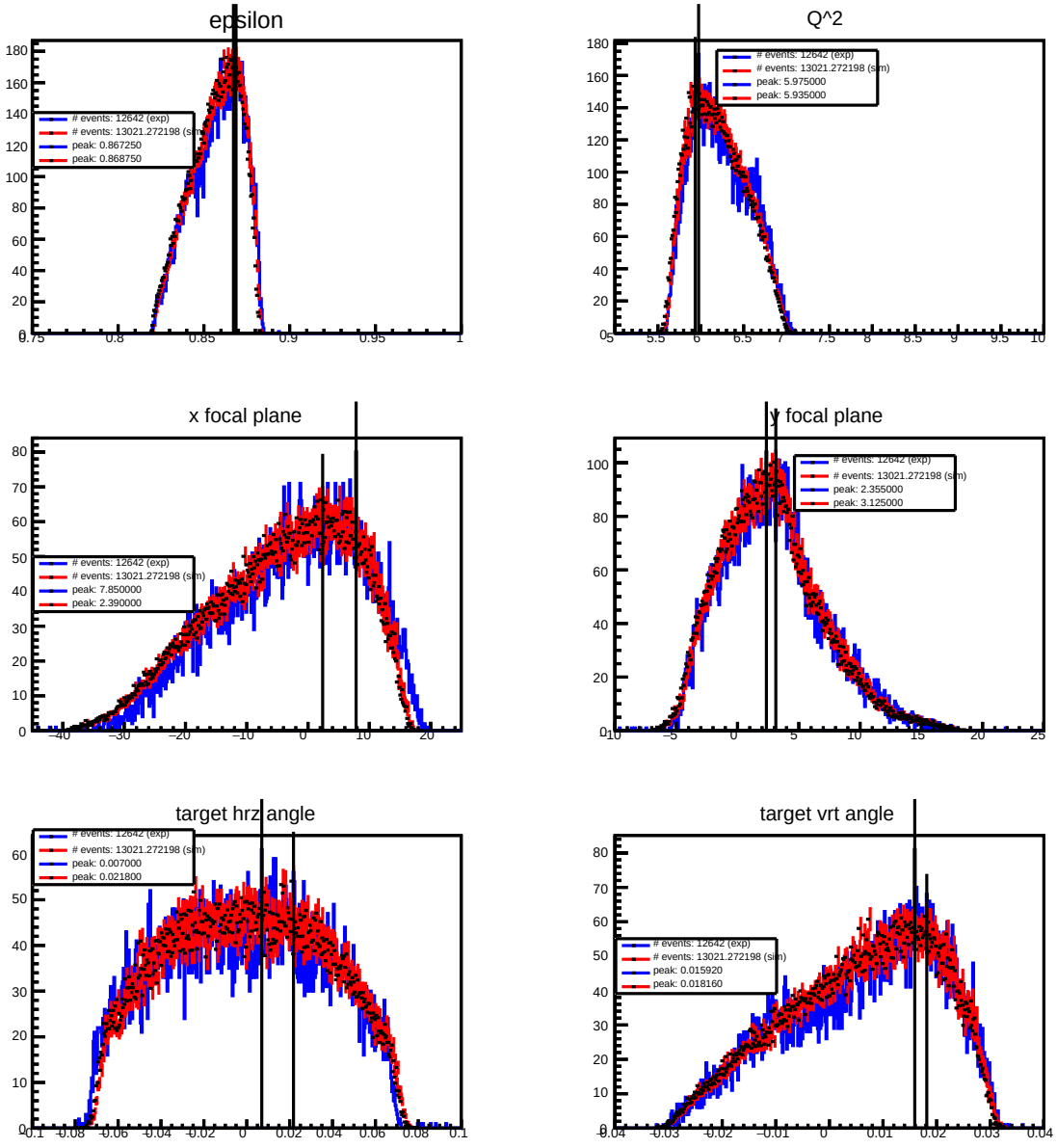

Figure 4.8: Multiple variables shown with experimental (blue) and SIMC (red) results overlayed with cuts applied (Run 12080)

These results show that the elastic cross section for the Pion LT experiment is within 10% of the expected value, and has successfully been verified.

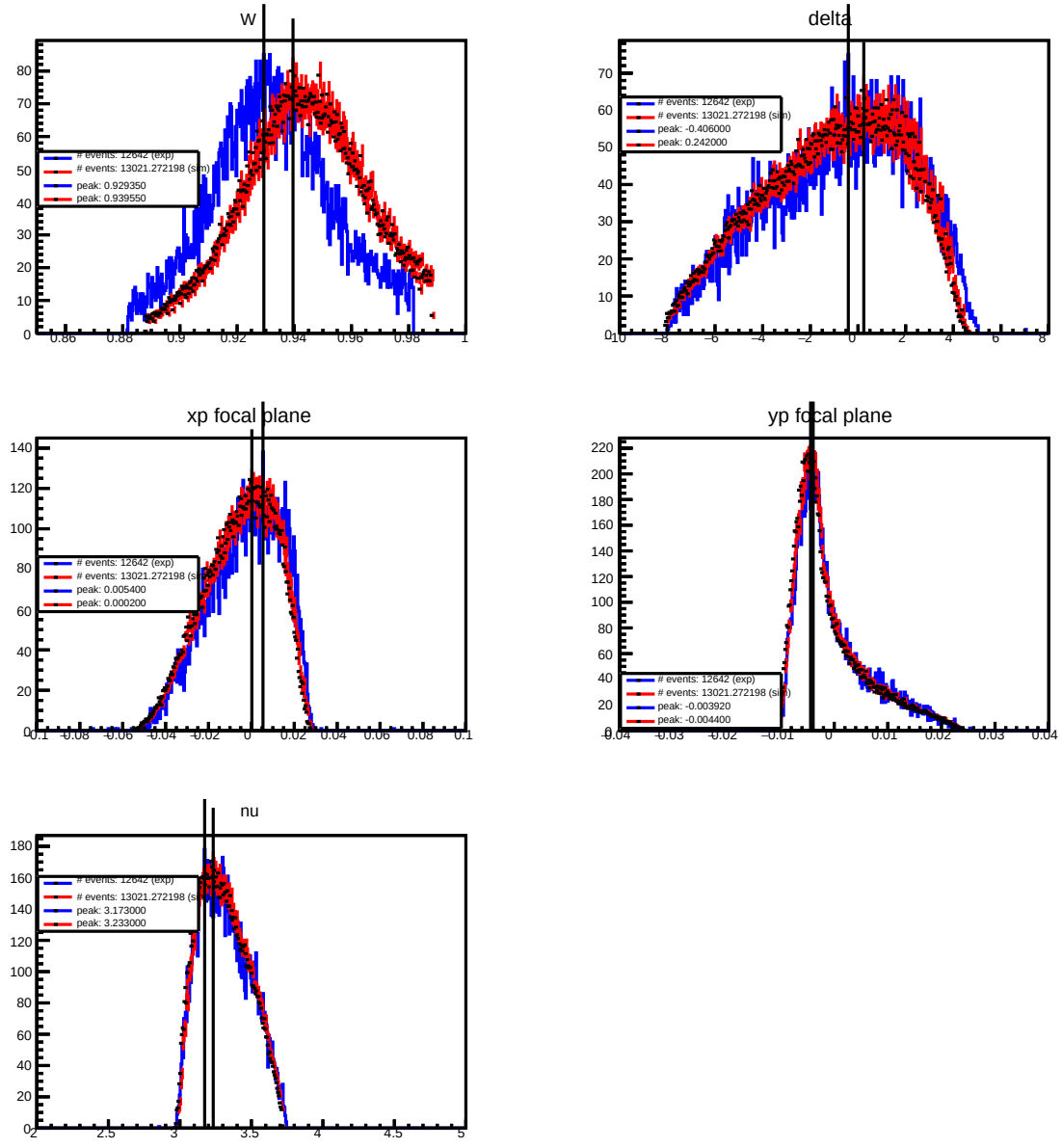

Figure 4.9: More variables shown with experimental (blue) and SIMC (red) results overlaid with cuts applied (Run 12080)

			Expected cross section		
Run Number	θ (deg)	E (GeV)	Rosenbluth (cm^2) Point-like	SIMC (cm^2) Extended Target	% Effect
12080	19.880	9.158	2.76×10^{-35}	2.81×10^{-35}	1.76
12083	19.880	9.158	2.76×10^{-35}	2.81×10^{-35}	1.77
13854	19.885	7.913	8.29×10^{-35}	8.83×10^{-35}	6.52

Table 4.4: Comparison of the Rosenbluth and simulated cross sections. E is the beam energy and θ is the scattering angle.

5 Conclusions

This analysis aimed to verify the elastic cross section from the Pion LT experiment run in 2021-2022 at Jefferson Lab. By using ROOT to filter for good elastic data, and configuring SIMC to create events that matched those kinematics, the elastic cross section was able to be extracted. The results of this analysis showed that the elastic cross section was verified to 10% of the expected value. This is within the target range we aimed for when the analysis started. These results can now aid in the reliability of other data taken for this experiment.

To further decrease the difference between the expected model results and experimental results, other techniques not applied here could be implemented in the future. Some of these considerations include: detector efficiency and simulation of the solid angle.

References

[1] B. Povh, M. J. Lavelle, K. Rith, C. Scholz, and F. Zetsche, *Particles and Nuclei: An Introduction to the Physical Concepts*, 6th ed. Springer, 2006.

[2] J. Lab, "Timeline." [Online]. Available: https://www.jlab.org/about/visitors/history

[3] ——, *JLab Aerial Photo*. flicker.com/photots/jeffersonlab, Apr 2012.

[4] M. Defurne *et al.*, "A glimpse of gluons through deeply virtual compton scattering on the proton," *Nature Commun.*, vol. 8, no. 1, p. 1408, 2017.

[5] J. Murphy, *APS April Meeting 2022*. APS, 2022. [Online]. Available: https://meetings.aps.org/Meeting/APR22/Session/Q13.1

[6] Z. Ye, J. Arrington, R. J. Hill, and G. Lee, "Proton and Neutron Electromagnetic Form Factors and Uncertainties," *Phys. Lett. B*, vol. 777, pp. 8–15, 2018.

[7] "Accelerator Science." [Online]. Available: https://www.jlab.org/accelerator

[8] C. H. Rode and J. . G. P. Team, "Jefferson Lab 12 GEV CEBAF Upgrade," *AIP Conference Proceedings*, vol. 1218, no. 1, pp. 26–33, 04 2010. [Online]. Available: https://doi.org/10.1063/1.3422362

[9] J. Lab, "Jefferson Lab Factsheet," 2016. [Online]. Available: https://www.jlab.org/sites/default/files/2016jlabfactsheet.pdf

[10] M. Dlamini, "Measurement of Hard Exclusive Electroproduction of Neutral Meson Cross Section in Hall A of JLab with CEBAF at 12 Gev," Ph.D. dissertation, Ohio University, 2018.

[11] S. Glamazdin and R. Pomatsalyuk, "Moller Polarimetry for DVCS," Jan 2017. [Online]. Available: https://indico.jlab.org/event/197/contributions/1667/attachments/1458/1897/Moller_for_DVCS.pdf

[12] S. A. Wood, H. C. Staff, and Users, "2019 Version: Jefferson Lab Hall C Standard Equipment Manual," 2019.

[13] H. Mkrtchyan and R. Carlini, "The Lead-Glass Electromagnetic Calorimeters for the Magnetic Spectrometers in Hall C at Jefferson Lab," *Jefferson Lab*, p. 2, 2012.

[14] O. Benhar, D. day, and I. Sick, "Inclusive Quasi-Elastic Electron-Nucleus Scattering," *Rev. Mod. Phys.*, vol. 80, pp. 189–224, 2008.

[15] C. Yero, "Cross Section Measurements of Deuteron Electro-Disintegration at Very High Recoil Momenta and Large 4-Momentum Transfers (Q^2)," Ph.D. dissertation, Florida Intl. U., Florida Intl. U., 2020.

[16] K. Bishnu, "Deep Exclusive π_0 Electroproduction Measured in Hall A at Jefferson Lab with the Upgraded CEBAF," Ph.D. dissertation, Ohio University, 2020.

[17] [Online]. Available: https://coda.jlab.org/drupal/

[18] R. team, "Analyzing Petabytes of Data, Scientifically." [Online]. Available: https://root.cern.ch/

[19] J. Bericic, "Notes on HMS_OPTICS," March 2017. [Online]. Available: https://hallcweb.jlab.org/DocDB/0008/000849/001/HMS_optics_notes.pdf

[20] J. Lab, "Jefferson Lab Electronic Logbook." [Online]. Available: https://logbooks.jlab.org/book/hallc

[21] ——, "SIMC - Physics Monte Carlo for Hall C and Hall A," 2008. [Online]. Available: https://github.com/JeffersonLab/simc_gfortran

[22] A. C. I. for Nuclear Physics. [Online]. Available: https://kinematics.kph.uni-mainz.de/

[23] J. Roche, *HMS Extended Target*, 2024.